

# Experiments and identification of thermoacoustic instabilities with the Rijke tube

Andrea Iannelli<sup>1</sup>, Martin Stefan Baumann<sup>2</sup>, Samuel Balula<sup>1</sup> and Roy S. Smith<sup>1</sup>

**Abstract**—This paper is concerned with the experimental characterization of a thermoacoustic demonstrator known as the Rijke tube. An approach which leverages the prior qualitative knowledge of the system’s behaviour to plan the experiment campaign and identify reliable models of the system is described. First, nonlinear features of the dynamics, e.g. the type of Hopf bifurcation triggered by the thermoacoustic coupling and the periodic orbits arising from it, are investigated. Then, a family of linear systems, parameterized with a coefficient related to the heat release, is constructed. Different approaches for input design and identification are tested. The results show that the identified models can favourably complement the prior knowledge gained from first principles and provide quantitative assessments on the linear and nonlinear behaviour of the system.

## I. INTRODUCTION

Thermoacoustics studies the dynamic interaction between pressure and heat transfer [1]. An example of these phenomena is represented by thermoacoustic instabilities, where acoustic waves adversely couple with unsteady heat release determining loss of stability in the form of self-sustained periodic responses, or Limit Cycle Oscillations (LCO). This problem is particularly relevant in jet engines and gas turbines, where acoustic pressure amplitudes reaching 10% of the mean operating pressure are not uncommon. As a result, research in this domain has largely focused on finding ways to passively or actively suppress these behaviours [2]. However, from an energy harvesting perspective, thermoacoustic LCO are a prospective green energy resource. Indeed, one can think of extracting the mechanical power from the heat-excited waves and convert it into electricity or directly use it to drive other machines. Active control represents then a possible key enabler since, depending on the objective, it can increase performance and efficiency of heat-driven thermoacoustic machines.

Great attention has therefore been devoted to modeling these phenomena. Depending on the purpose of the model, different directions have been taken. For prediction purposes only, e.g. determine the range of operating conditions for which LCOs arise, first principles models are typically considered. These are obtained

from the fluid and heat release dynamics and their nonlinear coupling, described by complex nonlinear partial differential equations [3]. In addition to their potential robustness issues due to modeling assumptions and non-exact parameters knowledge, the complexity of these models are not amenable for control design purposes. Most of the literature for control-oriented models has considered a simplified representation consisting of a linear single harmonic acoustic field coupled with the heat release modelled as a static delayed saturation-like nonlinearity [4]. While this schematization is sufficient to justify the presence of LCO and capture the main features, other research has suggested that it might not be exhaustive [5]. Modeling, and its closely related task of identification, of thermoacoustic instabilities is thus an active area of research.

In this paper, the Rijke tube [6], a vertical tube with a heater inside and equipped with microphone and speaker, is used as laboratory test bed of thermoacoustic instability. The aim is to show the potential of system identification [7], when informed by first principles modeling, to provide thermoacoustic models which achieve the trade-off between complexity and reliability highly desirable in models for control. After describing the configuration and introducing the thermoacoustic problem in Section II, important considerations concerning experiment design and system identification, and representing the basis for the studies reported in the paper, are discussed in Section III. Section IV reports a set of experiments aimed at characterizing the nonlinear response of the system. As the amount of heat released in the tube is increased, the system undergoes a Hopf bifurcation [8] above which the equilibrium loses stability and self-sustained oscillations are clearly audible. As known from the literature [6], a proportional controller sensing pressure at the top of the tube and actuating a speaker at the bottom, is able to damp out the oscillations. An important new finding discovered here is that, for a fixed value of the current, the tube undergoes a subcritical Hopf bifurcation as the controller gain is changed. Section V focuses on the identification of a family of LTI models linearized about the branch of (stable and unstable) equilibria. For the latter, a closed-loop setting has to be used to first stabilize the plant and then identify it. Different options for the identification algorithms and input design are presented and the results are critically discussed.

\*This work is supported by the Swiss National Science Foundation under grant no. 200021\_178890.

<sup>1</sup> Andrea Iannelli, Samuel Balula and Roy S. Smith are with the Automatic Control Lab, ETH, Zürich 8092, Switzerland [iannelli/balula/rsmith@control.ee.ethz.ch](mailto:iannelli/balula/rsmith@control.ee.ethz.ch)

<sup>2</sup> Martin Stefan Baumann is with TU Wien, Karlsplatz 13, 1040 Wien, Austria [e1527563@student.tuwien.ac.at](mailto:e1527563@student.tuwien.ac.at)

## II. BACKGROUND MATERIAL

This section provides a description of the experimental setup (Section II-A) and an overview of approaches to the modeling of thermoacoustic instabilities (Section II-B).

### A. Experimental setup

The Rijke tube is a thermoacoustic resonator consisting of a straight cylindrical tube with two open ends and a heat source (typically an electrical resistance) inside. For values of the electrical current  $I_w$  in the resistance above a critical threshold value, the tube starts generating a clear humming sound. This is the manifestation of self-sustained pressure oscillations caused by the interaction between the heat release and the acoustic field. In particular, the phasing between the gas pressure and velocity in the region of the heat source must be such that heat is added to (extracted from) the gas at the moment of greatest compression (rarefaction), satisfying in this way the Rayleigh criterion for the development of heat-driven acoustic oscillations [9].

Due to its simplicity, the Rijke tube has been used as a prototype of thermoacoustic instabilities to enable a cheap and safe testing of dedicated modeling and control strategies [9], [6]. The configuration employed here also includes a microphone, which measures the pressure  $p_m$  at 95% height of the tube, and a loudspeaker at the lower end to generate an exogenous sound pressure  $p_s$ . In order to perform system identification, possibly in closed loop, data acquisition of these signals and real time control were performed with a dedicated control signal generator and data acquisition system (in the following termed CDAQ) developed in-house. Details of the hardware and software parts of the CDAQ are available in [10]. Figure 1 presents a schematic of the apparatus used in this work. The tube is mounted in vertical position, which guarantees the presence of a mean buoyancy flow around the heat source (in some experiments the tube can be found horizontally and the mean flow is provided with an external fan [11]), and has a total length,  $L_t$ , of 120 cm and an inner radius of 3.65 cm. The heat source consists of three wires each with a resistance of  $5 \frac{\Omega}{\text{m}}$  and a length of 1 m. The wires are coiled and placed side by side to ensure that the heat source operates homogeneously over the cross-sectional area of the tube at a specific height.

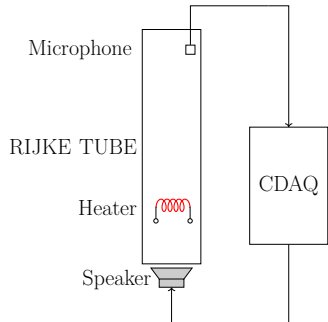


Fig. 1: Experiment configuration.

### B. First principles models of thermoacoustic instabilities

Modeling thermoacoustic instabilities is a challenging task due to the complexity of the phenomena involved [1]. On the one hand, the thermodynamic variables (e.g. pressure, velocity) are described by nonlinear partial differential equations (PDEs). On the other hand, describing the heat release, and its coupling with the thermodynamics variables, is a complex task, especially when heat originates from combustion [3].

The Rijke tube is an instructive example as it allows important simplifications in the modeling while retaining the main physical features. The equations governing the thermodynamic variables (namely density  $\rho$ , pressure  $p$  and velocity  $u$ ) consist of the mass, momentum and energy balances (Euler equations) plus the state equation [6]. By exploiting the rotational symmetry and the high aspect ratio of the tube in the axial direction  $x$ , the hypothesis of one-dimensional flow can be made. The corresponding set of 1D nonlinear PDEs can then be linearized about a steady-state solution ( $\bar{\rho}, \bar{p}, \bar{u}$ ) and the perturbation dynamics in terms of ( $\tilde{\rho} = \rho - \bar{\rho}$ ,  $\tilde{p} = p - \bar{p}$ ,  $\tilde{u} = u - \bar{u}$ ) is studied. Since the flow conditions are subsonic inside the tube,  $\bar{u} \cong 0$ , and as a result the mass equation is decoupled from the others. Therefore, the variable  $\tilde{\rho}$  can be dropped. The resulting set of 1D linear PDEs represents a wave equation:

$$\begin{aligned} \bar{\rho} \frac{\partial \tilde{u}}{\partial t} + \frac{\partial \tilde{p}}{\partial x} &= 0, \\ \frac{\partial \tilde{p}}{\partial t} + \gamma \bar{p} \frac{\partial \tilde{u}}{\partial x} - (\gamma - 1)Q(\tilde{u}_w)\delta_D(x - x_w) &= 0, \end{aligned} \quad (1)$$

where  $\gamma$  is the ratio of specific heats of the gas,  $\delta_D$  is the Dirac delta function,  $x_w$  is the axial location of the wire and  $Q$  is the heat released from the wire acting as source term in the energy balance. The latter is a nonlinear function of the perturbed gas speed at the wire location  $\tilde{u}_w$ , and its modeling is key to capture the nonlinear response of the system. Note also that (1) should be equipped with initial and boundary conditions (the latter might account for control inputs when these are employed). Since the heat source is a hot wire, King's law can be employed for this purpose [6]. This provides an expression of the heat transfer as a function of conduction and convection contributions:

$$Q = L_w(k_1 + k_2\sqrt{|\tilde{u}_w|})\Delta T, \quad (2)$$

where:  $L_w$  is the length of wire;  $k_1$  and  $k_2$  are respectively conduction and convection constants empirically determined and depending on several factors including geometry and thermal properties (e.g. they will be proportional to the current  $I_w$  circulating into the wire);  $\Delta T$  is the difference between the wire and unperturbed gas temperature. It is apparent from (2) that the convection is proportional to the speed of the gas near the flame, but this relationship is not linear, with this amplification factor decreasing as the speed increases. This saturation effect is the key element triggering limit cycles and is

also common in combustion-driven instabilities, where the concept of flame describing functions is commonly used [12], [13]. Observe that (2) is a static map between gas speed and heat release. However, in the presence of gas fluctuations, dynamic effects in the thermoacoustic coupling will not be negligible. It has been observed that the main effect is a time lag  $\tau$  between  $Q$  and  $\tilde{u}_w$ , and so  $\tilde{u}_w(t - \tau)$  should be considered in (2) [11].

### III. SYSTEM IDENTIFICATION APPROACH

Models relying on first-principles are likely to suffer from two shortcomings. There is a potential issue of robustness, e.g. the modeling assumptions might not be correct and the value of some parameters might only be approximately known. Secondly, the size and complexity of the models might make them intractable for control design. System identification is employed here to overcome some of these issues by identifying models from experiments while also exploiting prior knowledge of the system gathered from first principles modeling. This complementarity will be discussed in this section.

It is clear that the current  $I_w$  circulating in the wire (which is proportional to the heat released into the tube) is a fundamental parameter for the dynamics of the plant. There is a threshold value  $I_w^{cr}$  below which the system is at equilibrium and thus linearizing the original nonlinear PDEs about ambient conditions in the range  $I_w \in [0, I_w^{cr}]$  leads to a wave equation in the domain  $x \in [0, L_t]$  with the heat source term at  $x = x_w$ . Its solution consists of two pressure waves originating in the coil and travelling in opposite directions, which after refraction at the ends give rise to a standing wave in the tube. Solving the wave equation thus involves finding the functions  $\tilde{p}(x, t)$  and  $\tilde{u}(x, t)$  representing the amplitudes of the wave at any position  $x$  and time  $t$ . A possible model structure for the identification of the plant in this regime is that of a family of linear time-invariant (LTI) systems (parametrized with the current  $I_w$ ) where the states represent the *modes* of the waves. Since the underlying dynamics are infinite dimensional, the order of the LTI is not known a priori and the energy content associated with each mode, identifiable in the experiments, can be used as criterion to truncate the LTI order. Each mode is known to have a pair of complex conjugate eigenvalues with harmonically related frequencies  $\omega_k = k \frac{c\pi}{L_t}$  ( $c$  is the speed of sound) and real part depending on the damping of the system. Note that  $\omega_1$  is expected to be close to the fundamental frequency of oscillation of a tube open at both ends, namely a half-wavelength standing wave. Indeed, for the experimental setup used in this work  $\omega_1 = 898 \frac{\text{rad}}{\text{s}}$  and  $f_1 = \frac{\omega}{2\pi} = 142.9$  Hz, which corresponds to a wavelength  $\lambda = \frac{c}{f_1}$  equal to twice the length of the tube. This information gives important indications (e.g. frequency resolution and frequency range of interest) for the input design identification experiments. As for the damping, this is not usually considered in the first principle equations (1), since its sources are difficult to

model, but it is very important to correctly determine the onset of self sustained oscillations.

As  $I_w$  increases beyond  $I_w^{cr}$ , the tube starts producing a steady humming sound generated by the pressure oscillations. This is due to a Hopf bifurcation at  $I_w^{cr}$  where the branch of equilibria associated with the LTI system discussed above loses stability and a branch of LCO emanates. This requires a radical change in the identification approach to be used in the range  $I_w > I_w^{cr}$ . Since the system is now in a nonlinear regime, if the goal is to provide a linear characterization then the steady state about which the model is linearized should be defined. Indeed, for each value of  $I_w$  there is a stable periodic orbit and an unstable equilibrium. In an open-loop experiment, only stable steady states can of course be observed. This consists of an LCO, hence the associated model structure is a linear time-periodic (LTP) system, describing the behaviour of the system around this attractor, and system identification methods for this class of systems [14] could be adopted for that purpose. The approach taken here (Section V) is to first stabilize the response with a controller and then identify the associated closed-loop stable plant and, from this, the (unstable) open-loop plant. Note that, while the model structure is here unchanged with respect to the case of  $I_w \in [0, I_w^{cr}]$ , the identification approach should change as experiments are now done in closed-loop [7].

An alternative approach consists of identifying directly a nonlinear system which captures the different attractors in the system. The underlying nonlinear PDE, or a reduced order version of it, has to be identified from essentially periodic responses, leading to experiment design and identifiability difficulties. An incremental approach, investigated in Section IV, consists of identifying *features* of the nonlinear systems. Examples of these are the exact nature of the Hopf bifurcation (subcritical and supercritical), and the main properties of the response (the frequency content of the oscillations, and the effect of system parameters on it).

## IV. EXPERIMENTS ON THE RIJKE TUBE

### A. Characterization of the system's behaviour

Experiments for low values of the heater current (that is,  $I_w < I_w^{cr}$ ) have been first carried out. An example of the response in this regime ( $I_w = 8.4$  A) is presented in Fig. 2. The input signal (top), applied through the speaker, was constructed as the multiplication of two signals: a chirp sweeping the frequencies between 100 Hz and 1 kHz in 20 s, and an exponentially decaying signal (with time constant 4 s). The output signal (bottom), measured by the microphone, shows peaks caused by the excitation of the tube's modes. The output however decays to zero as the input signal vanishes, showing that the value of the current in the resistance is not high enough to trigger self sustained oscillations.

By increasing  $I_w$ , the damping of the system decreases and the critical current value  $I_w^{cr}$  at which the system

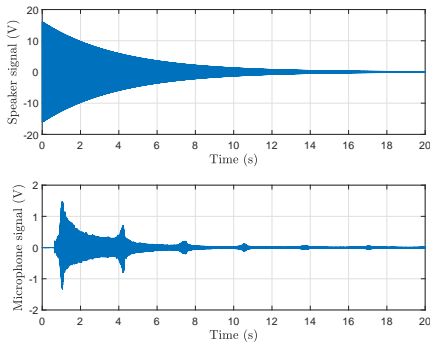


Fig. 2: Exponentially decaying chirp input and output of the tube at  $I_w=8.4$  A.

starts humming is reached, with the response converging to an LCO. The threshold value found in the experiments is approximately  $I_w^{cr} \approx 8.8$  A. Figure 3 shows the steady-state response of the system at 60 s for  $I_w=9.6$  A  $> I_w^{cr}$ . This experiment was performed with zero input signal, and thus shows that an infinitesimal perturbation in the environment is able to lead to an oscillatory response. The measured signal is converted from V to pressure units by using the gain factor of the microphone (see [10]) and pressure variations  $\tilde{p}$  are plotted.

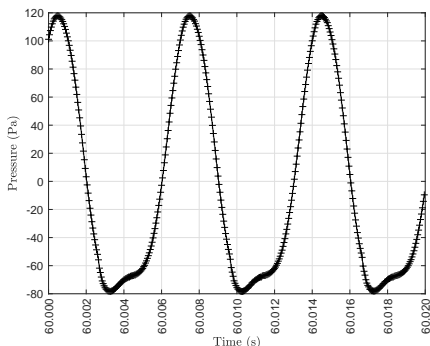


Fig. 3: Steady-state pressure oscillations  $\tilde{p}$  relative to the ambient pressure (for  $I_w=9.6$  A).

Once the bifurcation point and the existence of an LCO have been ascertained, a more quantitative characterization of the nonlinear response is performed by analyzing the frequency content of the oscillations. Figure 4 shows the power spectral densities (PSD) of the LCO for different heater currents. Those were obtained by averaging data measured at the steady state (as those in Fig. 3) and using Welch's method for the spectral estimate. The highest peak (at approximately 143 Hz), corresponds to the first resonant mode and is very close to the frequency  $f_1$  of the fundamental mode of the linearized system discussed in Section III. By closer inspection it can be observed that the peak frequency shifts towards higher frequencies with increasing heat, in particular for 9.6 A, 10 A, and 11 A the highest peak is at 142.7 Hz, 143 Hz, and 143.9 Hz respectively. The other peaks occur at approximately multiples of the fundamental frequency and correspond to higher modes.

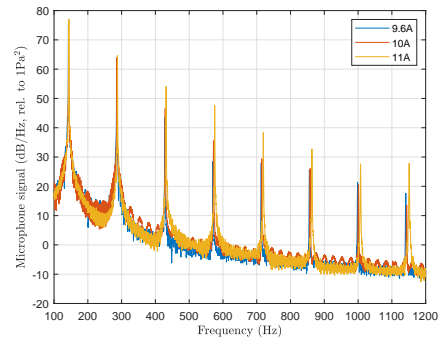


Fig. 4: PSD of the LCO for different heater currents.

### B. Control for stabilization and periodic orbit tracking

A feedback controller, measuring pressure and actuating the speaker, is then implemented in the CDAQ (Fig. 1) with a twofold aim. Firstly, a controller is needed to identify the LTI systems associated with the branch of unstable equilibria. Indeed, it is known from the literature [6] that a proportional controller  $K_c$  (with positive feedback) is sufficient to damp out the oscillations. Secondly, since the controller has a simple architecture, it is possible to use the gain  $K_c$  as bifurcation parameter and track the periodic orbits experimentally.

In Fig. 5 the effect of a proportional controller on the LCO response at 9.6 A for different values of  $K_c$  is investigated. Starting from a pre-existing steady state oscillation (i.e. the one in Fig. 3), the controller is activated at time 1 s, and the envelopes of the maximum and minimum of the signals for 4 values of  $K_c$  are plotted. While the effect of  $K_c = 0.072$  is only to decrease the LCO amplitude,  $K_c = 0.144$  features a slowly decaying response, and the other two gains successfully achieve convergence to a stable equilibrium.

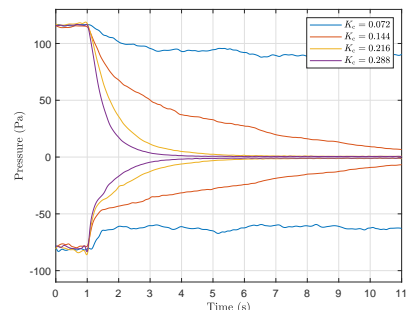


Fig. 5: Effect of the controller gain  $K_c$  on the envelope of the LCO at  $I_w=9.6$  A.

Tracking of the LCO with respect to the parameter  $K_c$  is performed by exploiting the capability of the CDAQ to adjust the controller in real time and with very fine increments. In other words, by using  $K_c$  as bifurcation parameter, *experimental continuation* of the system is performed, which represents a conceptually equivalent analysis to the one done with numerical continuation [8] when a model is available. At a current of 9.6 A, starting from a gain of  $K_c = 0$  (i.e. open loop conditions), the gain is first increased up to  $K_c = 0.2$  and then decreased

back to  $K_c = 0$ . Figure 6 shows for  $K_c \in [0.05, 0.14]$  the *experimental bifurcation plot* in terms of maximum and minimum of the envelope of  $\tilde{p}$ .

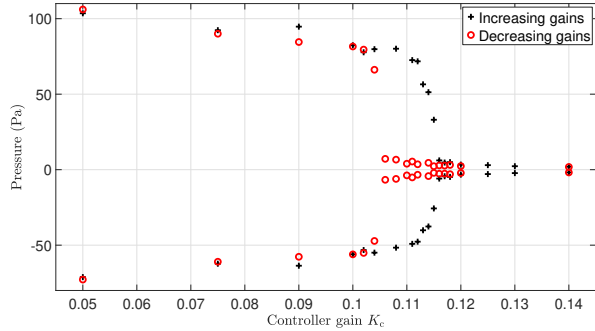


Fig. 6: Experimental bifurcation plot.

Two distinct branches can be observed. The one denoted by the black marker  $+$  indicates datapoints that were obtained by increasing the gain. It can be observed that the amplitude decreases as the gain is increased and for  $K_c > 0.115$  the LCO has practically disappeared. The second family of branches, denoted by the red marker  $\circ$ , is obtained starting the experiment at  $K_c = 0.2$  and then decreasing the gain. In this case the branch of equilibria remains stable until  $K_c = 0.106$ , below which the system exhibits an oscillatory response. The evident hysteresis points out that the system undergoes a subcritical Hopf bifurcation at  $K_c = 0.106$ . While it is known that thermoacoustic instabilities (and the Rijke tube in particular [11]) are prone to subcritical Hopf bifurcations with respect to parameters related to the heat exchange (e.g. the current  $I_w$ ), to the best of the authors knowledge, a similar behaviour with controller gains has not been shown previously. This is a very important aspect since subcritical Hopf bifurcation are notoriously more dangerous in applications than supercritical ones, being associated with bi-stable regions in the bifurcation parameter space [8], [15]. In the context of control of thermoacoustic instabilities, these results show that it is important to characterize, both numerically and experimentally, the nonlinear behaviour with respect to both the controlled and open-loop parameters of the system. The bi-stability is demonstrated in Fig. 7, where the measured responses at  $K_c = 0.112$  for the two different branches are plotted.

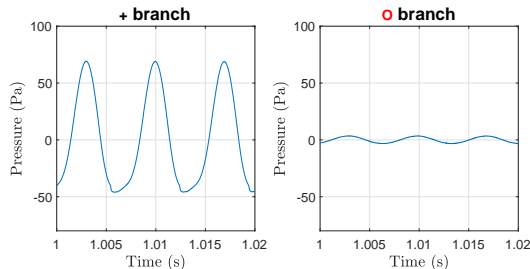


Fig. 7: Bi-stable response at  $K_c = 0.112$ .

## V. IDENTIFICATION OF LTI MODELS

In this section, linear system identification techniques are employed to identify the family of LTI models associated with the thermoacoustic equations (1)-(2) as the current in the resistance is varied. While in [6] identification of linear models for the Rijke tube has been previously carried out, here different options for input design, closed-loop identification algorithms, and transfer function realizations are investigated.

For values of  $I_w$  above the critical threshold the branch of equilibria about which the system is linearized loses stability and for identification it has to be stabilized. Therefore, closed loop system identification has to be performed for  $I_w > I_w^{cr}$ , while below the critical current open loop identification can be used.

The block diagram in Fig. 8 illustrates the signal and block interconnections conceptually describing the experiments. The transfer function from the speaker voltage  $u$  to microphone voltage  $y$  is denoted by  $G$  and is the object of the identification. The plant  $G_1$  includes also the gain of the power amplifier  $K_a$  and the signal conditioning gain  $K_s$  of the CDAQ, both known by the design of the control board [10]. Thus,  $G_1$  is the transfer function between the signals actually measured in the CDAQ. The reference signal  $r$  is used for identification purposes, while  $K_c$  is the proportional controller used to suppress the LCO.

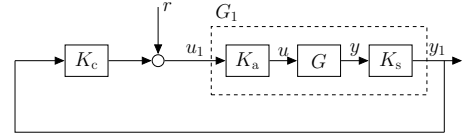


Fig. 8: Block diagram for identification.

For the reference signal  $r$ , Pseudo Random Binary Signals (PRBS) are a popular choice in experiment design ([7], Chapter 13). PRBS have the favourable feature, especially when identifying plants without much prior knowledge, of distributing an equal amount of energy over all the frequency spectrum (below the Nyquist frequency of the signal). The CDAQ has a sample rate of 20 kSamples/s, and thus a frequency resolution of 0.5 Hz was obtained with a PRBS-16 sequence, which is a periodic signal of period  $N = 2^{16} - 1 = 65535$  Samples  $\approx 3.21$  s. To improve the statistical properties of the estimates, 110 periods of this signal were used. The first 10 periods were discarded from each experiment to reduce the effect of transients and consequently decrease the bias error. The remaining 100 periods of data were then split into blocks of 10, that were averaged to result in one set of data containing only 10 periods (thus achieving a reduced variance error).

The empirical transfer function estimate (ETF), a nonparametric frequency-domain method for identification of linear systems ([7], Chapter 6), is used to identify the transfer function  $G$  for different values of  $I_w$ . In the

case of open-loop experiments (used to identify  $G$  for  $I_w < 8.6$ ), the estimate is straightforward:

$$\hat{G}(e^{j\omega}) = \frac{\hat{G}_1(z)}{K_a K_s} = \frac{1}{K_a K_s} \frac{Y_1(e^{j\omega})}{U_1(e^{j\omega})}, \quad (3)$$

where  $Y_1$  and  $U_1$  are the Fourier transforms of the signal  $y_1$  and  $u_1$ . In closed-loop experiments, the *direct method* in (3) is likely to provide inaccurate results as the measured output includes some noise which, due to the feedback, is correlated with  $u_1$ . To achieve a better estimate, two alternative techniques for closed-loop identification were tested ([7], Chapter 13). Both recast the problem as the identification of transfer functions for which the noise in the output is uncorrelated with the input. In the *indirect method*, the transfer function between the reference signal  $r$  and  $y_1$  is identified:

$$T_{y_1,r} = \frac{G_1}{1 + K_c G_1} = S G_1, \quad (4)$$

where  $S$  is the sensitivity function. Once an ETFE estimate for  $T_{y_1,r}$  is obtained, an estimate for the plant  $G$  can be obtained by inverting (4):

$$\hat{G}(e^{j\omega}) = \frac{\hat{G}_1(z)}{K_a K_s} = \frac{1}{K_a K_s} \frac{\hat{T}_{y_1,r}(e^{j\omega})}{1 - K_c \hat{T}_{y_1,r}(e^{j\omega})}. \quad (5)$$

A drawback of this method is that it requires perfect knowledge of the controller. The *joint input-output method* (used here unless otherwise stated) overcomes this issue by also considering the transfer function from  $r$  to  $u_1$ , i.e. the sensitivity function  $S$ . The new estimate, which no longer depends on the controller, can then be obtained as a ratio of the two ETFE:

$$\hat{G}(e^{j\omega}) = \frac{\hat{G}_1(z)}{K_a K_s} = \frac{1}{K_a K_s} \frac{\hat{T}_{y_1,r}(e^{j\omega})}{\hat{T}_{u_1,r}(e^{j\omega})} = \frac{1}{K_a K_s} \frac{S G_1(e^{j\omega})}{S(e^{j\omega})}. \quad (6)$$

Note that the latter method is also more robust to possible non ideal behaviours of some of the CDAQ internal components since it makes direct use of the measured signal  $u_1$ . A comparison of the estimate  $\hat{G}$  obtained with the two methods at a current of 9.6 A is shown in Fig. 9.

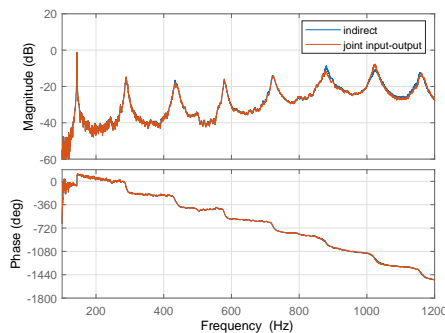


Fig. 9: Comparison of  $\hat{G}$  for the two closed loop identification methods at a current of 9.6 A.

The two methods are in very good agreement, which is expected since the controller here only consists of

a gain thus the *indirect method* should not encounter issues. Only at higher frequencies differences between the estimates can be noticed. This region is particularly sensitive to noise and thus the mismatch can be ascribed to it. Another interesting observation is that the identified transfer function highlights an instability of the first mode, which can be seen by the fact that the phase of the plant increases by approximately  $180^\circ$  at the resonance peak of the first mode. This is expected since the Rijke tube at  $I_w = 9.6$  A exhibited an LCO (Fig. 4). It is also noted the phase roll-off, from which an estimate of the time delay in the system, resulting from a combination of the delay in the CDAQ (known from its design) and the delay  $\tau$  in the heat equation (see end of Section II-B), can be obtained.

In order to improve the frequency resolution around the first mode (upon which the stability of the system depends), a linear chirp signal with a frequency sweep between 100 Hz and 200 Hz was used. The length of the signal was increased to 400 000 Samples per period (with the same sample rate) to have a frequency resolution of approximately 0.05 Hz. A similar pre-filtering of the identification signals, as used in the PRBS case, was employed. A comparison of the plant estimate with the two different input signals is shown in Fig. 10.

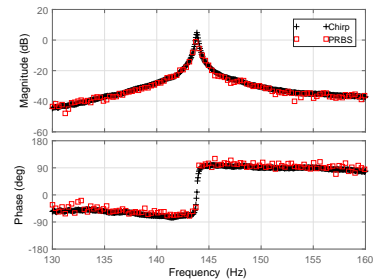


Fig. 10: Comparison of  $\hat{G}$  for different input at 9.6 A.

The estimate obtained with the chirp is smoother than the PRBS one (note that no smoothing is applied to the estimates). This is because the chirp has a higher power in this frequency range, reducing the variance of the estimates, and allowing the resonance peak, and the associated damping, to be better captured.

The identification strategy presented so far was repeated for different values of  $I_w$  to characterize the influence of this key parameter in the thermoacoustic coupling, and the results are shown in Fig. 11(a).

It can be concluded (especially from closeup of the phase plot in Fig. 11(b)) that 8.8 A is the critical value for the current. This is a confirmation of the experimental evidence gathered in Section IV-A, where the humming sound was only observed for currents above that value. In [6] it was noted that some estimates failed to capture the loss of stability of the plant (for values above  $I_w^{cr}$ ) due to the high precision required around the resonant peak to detect it. The identification strategy proposed here, consisting of mixed input signals, signals pre-filtering, no artificial smoothing and a more robust closed-loop

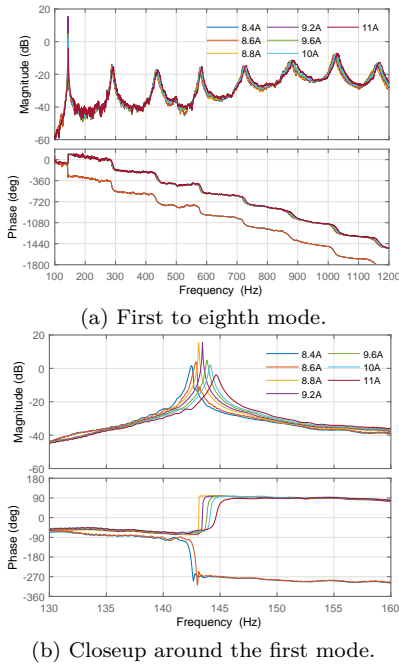


Fig. 11: ETFE  $\hat{G}$  for various heater currents.

identification algorithm, seems to overcome these issues. Another interesting aspect is the effect of  $I_w$  on the modal frequencies, which all slightly shift towards higher frequencies for increasing currents. The same trend was detected in Fig. 4 for the spectrum of the LCO.

Finally, for each of the identified ETFE a state-space model capturing the first 5 modes (i.e. 10 states) was constructed using frequency-domain subspace identification. A weighting emphasizing the frequency points around the resonance peaks was employed to obtain accurate results. In Fig. 12 the pole map of the first five modes as the current increases from 8.4 A to 11 A is plotted.

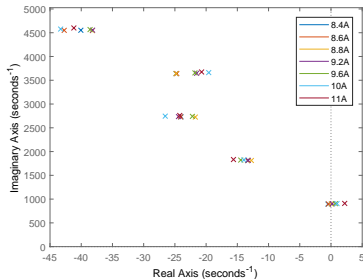


Fig. 12: Pole map of the family of state-space models.

The main effect of the parameter  $I_w$  is to move towards the right half plane the eigenvalues associated with the first mode, causing by doing so the unstable response discussed in Sec. IV and observed experimentally for  $I_w > 8.8$  A. The spectrum is that of a damped wave equation, where the imaginary part of the poles is an integer multiple of the fundamental frequency. As for the damping, it is observed that this increases for higher modes. While there exist damping models that mimic this effect [11] (by introducing a lumped damping parameter which is proportional to the frequency of the mode),

it is not common in the control literature to model damping in first-principles models (e.g. Eq. 1), despite its clear importance for the onset of thermoacoustic instability and thus active control applications.

## VI. CONCLUSIONS

The paper presents experiments and system identification results of a laboratory prototype of thermoacoustic instabilities. The nonlinear closed-loop response of the system is characterized in terms of LCO main features and onset of bifurcations with respect to a heat parameter and the controller gain. Once the dynamic response as a function of the current has been characterized, LTI systems describing the system around the branch of equilibria are identified. These models can be used to study the effect of macroscopic parameters (such as the amount of exchanged heat) on the spectrum of the system, and can be used to design controllers for active suppression or enhanced energy harvesting.

## REFERENCES

- [1] G. Swift, *Thermoacoustics*. Springer, 2007.
- [2] A. M. Annaswamy and A. F. Ghoniem, “Active control in combustion systems,” *IEEE Control Systems Magazine*, vol. 15, no. 6, pp. 49–63, 1995.
- [3] S. Roux, G. Lartigue, T. Poinso, U. Meier, and C. Bérat, “Studies of mean and unsteady flow in a swirled combustor using experiments, acoustic analysis, and large eddy simulations,” *Combustion and Flame*, vol. 141, no. 1, 2005.
- [4] A. Peracchio and W. M. Proscia, “Nonlinear heat-release/acoustic model for thermoacoustic instability in lean premixed combustors,” *J. Eng. Gas Turbines Power*, vol. 121, no. 3, pp. 415–421, 2001.
- [5] S. Savaresi, R. Bitmead, and W. Dunstan, “Non-linear system identification using closed-loop data with no external excitation: The case of a lean combustion chamber,” *International Journal of Control*, vol. 74, no. 18, pp. 1796–1806, 2001.
- [6] J. P. Epperlein, B. Bamieh, and K. J. Astrom, “Thermoacoustics and the Rijke Tube: Experiments, Identification, and Modeling,” *IEEE Control Systems Magazine*, vol. 35, no. 2, pp. 57–77, 2015.
- [7] L. Ljung, *System Identification: Theory for the User*. Prentice Hall PTR, 1999.
- [8] J. Guckenheimer and P. Holmes, *Nonlinear Oscillations, Dynamical Systems, and Bifurcations of Vector Fields*, ser. Applied Mathematical Sciences. Springer New York, 2002.
- [9] R. Raun, M. Beckstead, J. Finlinson, and K. Brooks, “A review of Rijke tubes, Rijke burners and related devices,” *Progress in Energy and Combustion Science*, vol. 19, no. 4, pp. 313 – 364, 1993.
- [10] (2018) Repository of PCB experiments. [Online]. Available: <https://gitlab.ethz.ch/andreaia/pcb-for-thermoacoustics>
- [11] M. Juniper, “Triggering in the horizontal Rijke tube: non-normality, transient growth and bypass transition,” *Journal of Fluid Mechanics*, vol. 667, p. 272–308, 2011.
- [12] N. Noiray, D. Durox, T. Schuller, and S. Candel, “A unified framework for nonlinear combustion instability analysis based on the flame describing function,” *Journal of Fluid Mechanics*, vol. 615, p. 139–167, 2008.
- [13] R. Smith, A. Banaszuk, and G. Dullerud, “Model validation approaches for nonlinear feedback systems using frequency response measurements,” in *IEEE Conference on Decision and Control*, 1999.
- [14] M. Yin, A. Iannelli, and R. S. Smith, “Subspace Identification of Linear Time-Periodic Systems with Periodic Inputs,” *IEEE Control Systems Letters*, 2020.
- [15] A. Iannelli, M. Lowenberg, and A. Marcos, “Computation of bifurcation margins based on robust control concepts,” *SIAM Journal of Applied Dynamical Systems*, 2020.